Megakaryocyte derived immune-stimulating cells regulate host-defense immunity against bacterial pathogens

Jin Wang[1#], Jiayi Xie[2,3#], Xue Han[2,#], Daosong Wang[3#], Minqi Chen[3], Linjia Jiang[2*], Meng Zhao[2,3,4*]

[1]Department of Endocrinology & Metabolism, The Third Affiliated Hospital, Sun Yat-sen University, Guangzhou, Guangdong, 510630, China

[2]RNA Biomedical Institute, Sun Yat-sen Memorial Hospital, Sun Yat-sen University, Guangzhou, Guangdong, 510120, China

[3]Key Laboratory of Stem Cells and Tissue Engineering, Zhongshan School of Medicine, Sun Yat-sen University, Ministry of Education, Guangzhou, Guangdong, 510080, China

[4]Lead Contact [#] These authors contributed equally to this work.

[*]Correspondence: Meng Zhao E-mail: zhaom38@mail.sysu.edu.cn;

Linjia Jiang: E-mail: jianglj7@mail.sysu.edu.cn

Abstract

Megakaryocytes (MKs) continuously produce platelets in bone marrow to support hemostasis. However, MKs also play roles beyond thrombopoiesis as they regulate hematopoietic stem cell quiescence and erythropoiesis, which suggests the functional heterogeneity of MKs. Here, using single-cell sequencing we identified an MK-derived immune-stimulating cell (MDIC) population, which plays an important role in host-protective response against bacteria. In contrast to platelet-generating MKs, MDICs highly express cell migration, immune-modulatory, and response genes. Upon *Listeria* (*L.*) *monocytogenes* infection, MDICs egress to circulation and infiltrate into the spleen, liver and lung. MDICs interact with myeloid cells to promote their migration and tissue infiltration. More importantly, MDICs stimulate phagocytosis of macrophages and neutrophils by producing TNFα and IL-6 and facilitating antigen-specific T cell activation via IL-6 to enhance anti-bacterial response. Ablation of MKs reduced innate immune response and compromised T cell activation in spleen and liver, impairs the anti-bacterial effects in mice under *L. monocytogenes* challenge. Finally, infection-induced emergency megakaryopoiesis efficiently stimulated MDICs generation upon bacterial infection. Overall, we identify MDICs as a novel MK subpopulation, which regulates host-defense immune response against bacterial infection.

Introduction

Megakaryocytes (MKs), a rare hematopoietic lineage in bone marrow, continually produce blood platelets to support hemostasis and thrombosis [1,2]. MK progenitors undergo multiple rounds of endomitosis during maturation to achieve polyploid [3-7] and migrate between distinct microenvironments and organs for their proliferation, maturation, and biological functions [8-14]. Although platelet generation is the prominent role of MKs, evidence suggests that MKs have other biological functions.

Mature MKs physically interact with hematopoietic stem cells (HSCs) and constitute a unique niche for HSC regulation in bone marrow. MKs produce multiple factors, including transforming growth factor-beta (TGFβ) [15,16] and platelet factor (PF4 or CXCL4) [17] to maintain HSC quiescence. MKs also interact with other niche cells, such as osteoblasts [18,19], non-myelinating Schwann cells [20,21], and blood vessels [8,22] to further influence the attraction and retention of hematopoietic stem and progenitor cells during homeostasis and stress. MKs express multiple immune receptors, including IgG Fc receptors, toll-like receptors (TLRs), major histocompatibility complex (MHC) [12,23-25], and produce numerous cytokines, such as PF4, TGFβ, IL-1, and IL-6, which regulate immune cell differentiation, survival, and migration [26-30]. These suggest that MKs might play roles in inflammation and infection [31-34]; however, the precise mechanism remains elusive.

Here, using single-cell RNA sequencing (scRNA-seq), we identified a novel immune-stimulating MK subpopulation, which participates in host defense against microbial pathogens.

Methods

Detailed descriptions of experimental methods are in Supplemental Methods.

Mice

C57BL/6-Tg(*Pf4-cre*)Q3Rsko/J (*Pf4-cre*), C57BL/6-Gt(ROSA) 26Sortm1(HBEGF)Awai/J (*iDTR*), C57BL/6-*Gt(ROS*A)26Sortm4(ACTB-tdTomato,-EGFP)Luo/J (*mTmG*), Gt(ROSA)26Sortm9(CAG-tdTomato)Hze (*tdTomato*) mice were obtained from the Jackson Laboratory. *Scl-CreER* mice were provided by J.R. Goethert. All mice were maintained in the C57BL/6 background. Animals were blindly included in the experiments according to genotyping results as a mix of male and female. All animal experiments were performed according to protocols approved by the institutional animal care and use committee.

Single cell RNA sequencing

Sorted $CD41^{+}FSC^{high}$ single cells from control mice and mice at three days after *L. monocytogenes* infection were processed through the Chromium Single Cell. Platform using the Chromium Single Cell 3' Library and Gel Bead Kit v3 (10X Genomics, PN-1000075) and the Chromium Single Cell B Chip Kit (10X Genomics, PN-1000074) as the manufacturer's protocol. In brief, over 7,000 cells of each sample were loaded onto the Chromium instrument to generate single-cell barcoded droplets. Cells were lysed and barcoded reverse transcription of RNA was occurred. Libraries were prepared by following amplification, fragmentation, adaptor, and index attachment, then sequenced on an Illumina NovaSeq platform.

scRNA-seq preprocessing

The scRNA-seq reads were aligned to the mm10 reference genomes, and unique

molecular identifier (UMI) counts were obtained by CellRanger 3.0.2. Normalization, dimensionality reduction and clustering were performed with the Seurat 3.0 R package [35] on RStudio. For control and *Listeria* (*L.*) *monocytogenes* infection group, we loaded one 10x Genomics well each and detected 5,663 and 5,948 cells which passed the cellranger pipeline, respectively. To ruled out potentially contamination, cells with >12% mitochondrial content or have <200 detected genes were excluded, with Seurat function subset (percent.mt<12 & nFeature_RNA>200). We ruled out doublets with default parameters of DoubletDecon R package, and 54 of control cells and 939 of *L. monocytogenes* infected cells were excluded. Following standard procedure in Seurat's pipeline, in combination with spearman correlation test and MetaNeighbor method, we obtain 3,272 MKs from control mice (1,712 MKs) and mice with *L. monocytogenes* infection (1,560 MKs) (3,897 and 3,449 immune cells were discarded respectively).

Data sharing statement

The scRNA-seq data generated in this study are deposited in GEO (GSE168224, https://www.ncbi.nlm.nih.gov/geo/query/acc.cgi?acc=GSE168224).

Results

Single-cell atlas identifies an MK-derived immunoregulatory cell population.

To explore the heterogeneity of MKs, we applied droplet-based single-cell RNA sequencing (scRNA-seq) with $CD41^{+}$ forward scatter $(FSC)^{high}$ MKs in bone marrow. To adequately enrich MKs at various stages, we gated over the top 1% of $CD41^{+}$ cells as described and combined transcriptomic analysis to capture sufficient and accurate MKs [36]

(Figure 1A; Supplemental Figure 1A-C). We successfully detected a total of 5,368 high-quality cells and excluded 3,656 immune cells according to their transcriptional profiles to obtain 1,712 MKs. MKs, with an average of ~4200 genes per cell, expressed MK-specific marker genes including *Pf4* and *Itga2b* (CD41) and exhibited high similarity to published megakaryocyte single-cell transcriptome rather than immune cells [36-38] (Figure 1B-D, Supplemental Figure 1D-M). MKs expressed higher mRNA and more genes than immune cells, presumably due to the polyploid of MKs [39] (Supplemental Figure 1N). Re-clustering 1,712 MKs revealed five clusters termed MK1 to MK5, each expressed MK marker genes (*Pf4*, *Itga2b*, *Vwf*, *Mpl*, *Itgb3*) and transcription factors required for MK differentiation (*Fli1*, *Nfe2*, *Gata1*, *Runx1*) and exhibited megakaryocyte transcriptional profiles compared to published data [36-38,40,41] (Figure 1B-D, Supplemental Figure 1O). Then we annotated these five clusters based on the feature genes of each cluster through enriched gene ontology (GO). MK1 highly expressed nuclear division genes, including *Mki67*, *Ube2c*, *Nuf2*, *Cdk1* [5,42,43] (Figure 1E-H), indicating endomitosis during MK polarization [2]. MK2 showed enrichment of genes related to DNA replication and repair genes such as *Mcm2*, *Ung*, *Cdca7*, *Mcm3* [44,45] (Figure 1E-H). MK3 contained feature genes associated with blood coagulation such as *Alox12*, *Gp6*, *Myl9*, *Thbs1* [46-49] (Figure 1E-H), indicating the role of platelet generation and thrombosis. MK4 exhibited B cell differentiation and antigen processing and presentation pathways, including feature genes *Cd74*, *H2-Aa*, *Ly6c2*, *H2-Eb1*, *S100a4*, *Ifi27l2a* and *Ctss* [50-53] (Figure 1E-H). MK5 enriched cell migration, immune-modulatory and inflammatory response genes, including cell migration genes *Ccl3*, *Ccl4*, *Ccl9*, *Cyp11a1*, *Cdh1*, *Cxcr4*, cytokine genes *Il6*, *Il15*, *Il18rap*, IgG Fc receptor gene *Fcer1a*, *Fcer1g*, and inflammatory response genes *Ier3*,

Cd200r3, *Junb*[54-63] (Figure 1E-H, Supplemental Figure 1P), indicating that this subpopulation might directly sense the immune signals to participate in immune responses [32]. Therefore, we referred this novel MK subpopulation as MK-derived immune-stimulating cells (MDICs). Interestingly, MDICs (MK5) exhibit a slightly lower expression of some canonical MK markers (*Vwf*, *Mpl*, *Itgb3*), transcription factors (*Gata1*), and a little higher expression of *Spi* (encoding PU.1), which is involved in immune cell differentiation, than other populations [64] (Figure 1C, Supplemental Figure 1P).

Overall, using scRNA-seq, we identified a new immune-stimulating MK subpopulation termed MDICs that might participate in cell migration, immune-modulatory functions, and inflammatory response.

MDICs migrate to peripheral organs upon *L. monocytogenes* infection.

To obtain purer MKs by CD41 markers through flow cytometry, we performed a tighter gating strategy than cell sorting for scRNA-seq to avoid $CD41^{-}$ cells containing immune cells. We further performed CD41 immunostaining to confirm the CD41 expression and polyploid in sorted MKs (Supplemental Figure 2A-B). Moreover, we seldom observed $CD41^{+}$ hematopoietic stem and progenitor cells (HSPCs) with a tighter gating strategy because of lower CD41 levels in HSCs, consistent with single-cell analysis showing rarely expressed HSC marker genes in MKs [65-68] (Supplemental Figure 1P, 2C). To assign the immune response and modulatory functionality to potential clusters, we identified surface protein and cytokinin encoded marker genes: *Cdh1* (encoding CD324/E-cadherin) and *Il6* enriched in MDICs (MK5), *Ccr2* enriched in MK4 and MDICs (MK5), and high

Cxcr4 expression in MDICs, compared to low *Cxcr4* level in classic MKs [69,70] (Figure 1G and I). Single cells expressed a high level of *Cxcr4* also enriched cell migration, immune-modulatory, and inflammatory response pathways (Supplemental Figure 1Q). Meanwhile, high levels of CXCR4 were associated with IL-6 labeled MDICs (MK5) according to flow cytometry (Supplemental Figure 2D), which indicated that high CXCR4 expression could be a potential marker to enrich MDICs. Indeed, MDICs (marked with $CXCR4^{high}$, hereafter) had smaller cell size and produced less platelets under Thrombopoietin (TPO) stimulation [71] (Supplemental Figure 2E). This showed that MDICs had distinct responses to TPO stimulation compared to classic MKs.

We further co-stained CD324, CCR2, or CXCR4 with CD41 in bone marrow cells from control mice and mice at three days after *Listeria* (*L.*) *monocytogenes* infection (Figure 2A), we found $CXCR4^{high}$ and $CD324^{+}$ MKs, but not $CXCR4^{low}$ and $CD324^{-}$ MKs, were reduced after infection without cell proliferation and apoptosis (28.8% and 30.5% decreased respectively, Figure 2B-F, Supplemental Figure 2F-H). However, $CCR2^{+}$ MK numbers did not show a significant change after infection in bone marrow (Supplemental Figure 2I-J). Note transcriptomic profiles showed that MDICs (MK5) enriched cell migration genes, including *Cxcr4* (Figure 1E, H, 2G). These results indicated that MDICs (MK5) might migrate in the bone marrow microenvironment or egress to circulation in response to infection. First, we explored the spatial distribution of MKs in bone marrow at three days after *L. monocytogenes* infection. Although HSCs are dramatically activated upon infection [72], we did not observe a significant influence of the association between MKs and HSCs upon *L. monocytogenes* infection (Figure 2H-I), albeit the critical role of perivascular MKs in maintaining HSC quiescence [15,17,73].

However, ~ 80% MKs directly contacted blood vessels three days after *L. monocytogenes* infection, which was 1.61-fold higher than control MKs (~ 40%) (Figure 2H, J, and Supplemental Figure 2K). Furthermore, significantly more CXCR4^{high} MKs contacted with blood vessels compared to CXCR4^{low} MKs after *L. monocytogenes* infection (1.23-fold increase; Figure 2K-L). In addition, we developed a live imaging method to trace MK migration in bone marrow (see Methods). Using *Pf4-cre*; *tdTomato* (tdT) reporter labeled MKs, we observed small MKs which did not rupture or release platelet rapidly migrated into sinusoid upon *L. monocytogenes* infection (Figure 2M, movie 1). Consistently, we found that CXCR4^{high} MKs increased in peripheral blood (3.04-fold increase, Figure 2N). However, CXCR4^{low} MKs did not differ at three days after *L. monocytogenes* infection (Supplemental Figure 2L). These results indicated MDICs might egress into circulation from bone marrow upon infection.

Accordingly, we observed a significant increase of CXCR4^{high} MKs in the liver (2.51-fold) and spleen (2.18-fold) at three days after *L. monocytogenes* infection (Figure 2O-P, Supplemental Figure 2M-N). To further investigate the migration of MKs into peripheral organs upon infection, we employed *Pf4-cre; Rosa26-cell membrane-localized tdTomato (mT)/ cell membrane-localized EGFP (mG)* (*R26R$^{mT/mG}$*) reporter mice, in which cell membrane-localized EGFP (mGFP) is expressed exclusively in MK lineage [74]. Using this reporter line, we found that mGFP^{+} MKs were dramatically increased in the liver (10.4-fold) and slightly increased in the spleen (1.29-fold, no significant difference) at three days after *L. monocytogenes* infection (Figure 2Q-R). To further confirm the infiltration of MDICs, we transplanted tdT^{+} bone marrow cells into recipients, which were infected by *L. monocytogenes* for one day (Supplemental Figure 2O). Interestingly,

we found that the majority of $tdT^{+}CXCR4^{high}$ MKs migrated into the liver (92.1%) and spleen (92.5%); however, much fewer $tdT^{+}CXCR4^{high}$ MKs migrated to bone marrow (33.3%) when tdT^{+} bone marrow cells were injected to recipients for two days (Supplemental Figure 2P). On the contrary, $tdT^{+}CXCR4^{low}$ MKs preferred migrating to bone marrow (66.7%) rather than the liver (7.93%) or spleen (7.53%) (Supplemental Figure 2P).

Overall, our data showed that bacterial infection increased the egressing MDICs in circulation, which might infiltrate into the liver and spleen, suggesting a role of MDICs in host-protective response in tissues.

MDICs promote myeloid cell migration upon *L. monocytogenes* infection.

Our scRNA-seq also revealed that MDICs (MK5) population highly expressed cell adhesion cell chemotaxis and myeloid cell activation genes compared to classic MK populations (Figure 1H, 3A). This indicated that MDICs might regulate immune cell chemotaxis, which is essential for host-defense response [75,76]. To test this, we performed an *ex vivo* transwell assay and found that $CXCR4^{high}$ MKs effectively promoted the mobilization of macrophages (2.50-fold), dendritic cells (1.99-fold), and neutrophils (1.87-fold), which was much more efficient compared to simultaneously purified $CXCR4^{low}$ MKs (Figure 3B-C). Consistently, MKs from the liver and spleen also efficiently promoted immune cell mobilization (Supplemental Figure 3A). However, CCR2 and CD324 could not enrich MKs that promote myeloid cell mobilization (Figure 3D, Supplemental Figure 3B). We noticed that MKs and myeloid cells were preferably trapped in the sinusoid (MK 2.33-fold, myeloid cell 2.95-fold increase) three days after *L.*

monocytogenes infection compared to control mice (Figure 3E-F). Moreover, the direct association between MKs, blood vessels, and myeloid cells increased (1.93-fold) in the bone marrow of mice three days after *L. monocytogenes* infection (Figure 3E, G). Moreover, we found that more than 2-fold myeloid cells were associated with CXCR4^{high} MKs in bone marrow compared to CXCR4^{low} MKs in mice at three days after *L. monocytogenes* infection (Figure 3H-I). Consistently, the myeloid cell-CXCR4^{high} MK association (mean distance 15.36 μm) was significantly closer than the myeloid cell-CXCR4^{low} MKs association (mean distance 25.62 μm, $p = 7.03\times10^{-4}$ by KS test, Figure 3J). Furthermore, bone marrow myeloid cells were found preferably adjacent to CXCR4^{high} MK-blood vessel intersection rather than CXCR4^{low} MK-blood vessel intersection in mice at three days after *L. monocytogenes* infection (Figure 3K). These observations indicated that CXCR4^{high} MKs might promote the tissue infiltration of myeloid cells to promote host-defense response.

To investigate the role of MKs in immune cell infiltration upon *L. monocytogenes* infection, we employed *Pf4-Cre; iDTR* mice, in which MKs were rendered sensitive to diphtheria toxin (DT) [15]. As four-time DT injections efficiently ablated MKs in bone marrow, we gave the *L. monocytogenes* challenge at the second DT injection and analyzed the immune response three days after infection (Figure 3L-M). MK ablation markedly increased the numbers of hematopoietic stem and progenitor cells in the bone marrow and peripheral blood as previously reported [15,77] (Supplemental Figure 3C-D). We also noticed an increase of innate immune cells (macrophages 2.04-fold, neutrophils 5.32-fold) in the bone marrow of MK ablated mice upon *L. monocytogenes* challenge (Figure 3N). However, MK ablated mice had dramatically reduced numbers of innate

immune cells in the liver (macrophage 44.4% decrease, DC 67.2% decrease) and spleen (monocyte 22.5% decrease, macrophage 40.0% decrease, DC 32.9% decrease, neutrophil 55.8% decrease) three days after *L. monocytogenes* infection (Figure 3O-P).

Overall, our observations indicated that upon *L. monocytogenes* infection, MDICs facilitated the infiltration of innate immune cells against bacterial infection.

MDICs enhance host-defense response against *L. monocytogenes* infection.

To characterize the role of MDICs in the bacterial clearance capability of myeloid cells, we co-cultured MKs with neutrophils or macrophages before phagocytosis assays. We found that CXCR4^{high} MKs efficiently stimulated the phagocytosis ability of neutrophils and macrophages against bacteria. CCR2^{+} MKs and CD324^{+} MKs also showed stimulation effects on macrophage phagocytosis (Figure 4A-D). Our scRNA-seq revealed that MDICs (MK5) population enriched cytokine production compared to classic MK populations (Figure 4E). We further explored the molecular insights of MDICs and found that CXCR4^{high} MKs highly expressed *Ccl6* (CCL6), *Tnf* (TNFα), and *Il6* (IL-6), which regulate inflammatory responses and immune cell proliferation [78,79 80] (Figure 4F). We further confirmed that more CXCR4^{high} MKs producing TNFα (4.08-fold) and IL-6 (6.96-fold) compared to CXCR4^{low} MK in mice with *L. monocytogenes* infection (Figure 4G, I). Consequently, higher protein levels of TNFα (3.80-fold) and IL-6 (6.11-fold) were observed in CXCR4^{high} MKs than CXCR4^{low} MKs, which is consistent with their phagocytosis promotion in mice with *L. monocytogenes* infection (Figure 4H, J). These suggested that MDICs might directly facilitate the host-defense response by producing TNFα and IL-6 to stimulate myeloid cell phagocytosis for bacterial clearance [78,79]. To test

this hypothesis, we investigated the role TNFα and IL-6 in the MDIC-stimulated phagocytosis ability of macrophages and neutrophils. We found that the CXCR4^{high} MK-stimulated bacterial phagocytosis abilities in macrophages and neutrophils were significantly compromised when TNFα or IL-6 were blocked by neutralizing antibody (anti-TNFα antibody: neutrophils 63.8% decrease, macrophages 51.6% decrease; anti-IL-6 antibody: neutrophils 46.7% decrease, macrophages 44.6% decrease; Figure 4K-N). This showed that MDICs promoted the phagocytosis function of neutrophils and macrophages by producing proinflammatory cytokine TNFα and IL-6. Consequently, *in vivo* the bacterial burdens were dramatically increased in the liver (81.2-fold), and spleen (1.93-fold) in MK ablated mice at three days after *L. monocytogenes* infection (Figure 4O-Q).

Overall, our data demonstrate that MDICs enhance innate immunity against *L. monocytogenes* infection.

Bacterial infection promotes coagulation and immune response in distinct MK subpopulations.

To explore the role of MDICs during pathogen infection, we further elaborated the single-cell transcriptional profile of MKs in mice at three days after *L. monocytogenes* infection (Figure 5A-D; Supplemental Figure 4A-B). We performed the low-quality cell filtration and immune cell removing using the same strategy as scRNA-seq in control MKs. *L. monocytogenes* infection stimulated the immune response and cytokine production genes in multiple immune cells (Figure 5C). We obtained 1,560 MKs from mice upon infection, which also presented five populations as in control mice and exhibited high correlation

with published MK transcriptome rather than immune cells (Figure 5D and Supplemental Figure 4C). MK1 and MK2 showed no significant changes in cell fractions, transcriptional profiles (Figure 5E, Supplemental Figure 4D), and the polyploid after infection (Supplemental Figure 4E). Platelet-generating MKs (MK3) and MK4 increased, whereas the MDICs (MK5) decreased (Figure 5E, Figure 2D) in infected mice compared to control mice. Platelet-generating MKs (MK3) enriched blood coagulation genes with a slight increase of immune response pathways upon *L. monocytogenes* infection (Figure 5F). MDICs (MK5) exhibited stimulation of immune response, especially interferon (IFN) signaling pathway and antigen processing and presentation, including elevated gene expression of *Ifitm3*, *Stat1*, *Bst2*, *Irgm1*, *H2-Q7*, *H2-Q6*, *H2-K1* [81-84] (Figure 5F-G), consistent with lung MKs [36,37]. As lung is an important site of platelet generation [12], we compared MK1 to MK5 with these published lung MK scRNA-seq datasets [36,37]. We found that MDICs (MK5) and platelet-generating MKs (MK3), which are involved in immunoregulatory and coagulation, showed greater similarity to lung MKs. (Figure 5H). MK5 also enriched genes involved in antigen processing and presentation pathway upon *L. monocytogenes* infection, in line with published lung MKs [36] (Figure 5I). Thus, bacterial infection stimulated platelet-generating MKs and activated immune-response MDICs.

Bacterial infection stimulates thrombopoiesis and T cell proliferation via MKs.

scRNA-seq analysis showed an increased platelet-generating MKs (MK3) ratio, indicating active thrombopoiesis upon *L. monocytogenes* infection to meet the demand of increased platelet consumption [85] (Figure 5E). In supporting this, more ruptured MKs

were observed in bone marrow three days after *L. monocytogenes* infection (Figure 6A-B). Consequently, platelets were quickly recovered during day 3 to day 7 post-*L. monocytogenes* infection (Figure 6C), although platelets were initially damaged upon acute infection [31,86].

Antigen processing and presentation pathway in MDICs was activated upon *L. monocytogenes* infection in scRNA-seq. We next asked whether MDICs regulate T cell response. Interestingly, we observed that CXCR4^{high} MKs efficiently promoted T cell proliferation (7.06-fold increase), which was more efficient than CXCR4^{low} MKs (4.70-fold increase; Figure 6D-E). Moreover, the CXCR4^{high} MKs, but not CXCR4^{low} MKs, induced T cell proliferation was significantly compromised (27.8% decrease) when IL-6 was blocked by neutralizing antibody (Figure 6E). This indicated that MDICs promoted T-cell proliferation by producing IL-6.

We further investigated the *in vivo* function of MKs in promoting adaptive immunity against bacterial infection. We used ovalbumin (OVA)-expressing recombinant microbe (*L. monocytogenes*-OVA$_{257-264}$) to infect control, or MK ablated mice (Figure 6F). At seven days after *L. monocytogenes*-OVA$_{257-264}$ infection, we found that MK ablation dramatically reduced OVA-specific T cells activation, in which the number of CD4^{+} IFNγ^{+} Th1 cells, CD4^{+}IL4^{+} Th2, and CD8^{+} cytotoxic T lymphocytes were markedly reduced (42.9%, 37.9%, and 57.4% decrease, respectively) in MK ablated mice, although the total numbers of CD4^{+} T cell and CD8^{+} T cells were not affected (Figure 6G and Supplemental Figure 5A, D). These observations of MDICs exhibited a similar ability to stimulate T cell activation through antigen processing and presentation to depend on MHC II after bacteria engulfment as previously reported in lung MKs [37]. Interestingly,

through tdTomato labeled MK transplantation, we found MKs more rapidly infiltrated into the lung upon *L. monocytogenes* (Figure 6H-J). These results indicated that immune-modulatory lung MKs shared similar functionality with MDICs.

MK-committed HSCs drive emergency megakaryopoiesis to replenish platelet consumption during acute inflammation [87]. We hypothesized that immune-modulatory MDICs might be derived from committed HSCs during *L. monocytogenes* infection. Using *Scl-creER*; *tdTomato*$^{+}$ reporter mice, in which HSPC promoted hematopoiesis can be traced through tamoxifen induction [21], we analyzed tdTomato labeled MKs and progenitors at 18 hours after infection (Figure 6K). We found that tdTomato^{+} MKs, including MDICs (CXCR4^{high}) and classic MKs (CXCR4^{low}), were increased upon infection (Figure 6L). However, progenitors were not significantly increased, consistent with previous report [87] (Figure 6M). This indicated that emergency megakaryopoiesis might participate in the defense against pathogens through producing MDICs.

Overall, our observation indicated that acute pathogen infection enhances thrombopoiesis and adaptive immune responses of MKs through inflammation-induced emergency megakaryopoiesis.

Discussion

MKs express multiple immune receptors, which participate in megakaryocyte maturation, platelet activation, and potentially influence neutrophils and the adaptive immune cells [32,88-90]. The expression of immune receptors might confer MKs with immune sensing capacity in inflammation and infection [32]. Accordingly, MKs prevent the spread of dengue virus infection by enhancing the type 1 interferons pathway in murine and clinical

biospecimens [91]. Recent scRNA-seq studies also suggested the existence of a potential immunoregulation subpopulation in MKs [37,92]. However, how MKs regulate host-defense response remains elusive. In our work, using scRNA-seq, we identified an immune-stimulating MK subpopulation, MIDCs, which highly expressed chemokine receptor CXCR4 and enhanced both native and adaptive immunity against bacterial infection.

Upon acute inflammation, platelet-generating MKs were consumed for platelet production [31]. Furthermore, CXCR4^{high} MDICs egressed into circulation and infiltrated into peripheral organs, such as the liver, spleen, and lung. This is consistent with previous reports that MKs egress and migrate to the pulmonary capillary [12,37,93], and CXCR4 navigates cell migration upon chemotactic stimuli [8,70]. HSCs like MK progenitors induce emergency megakaryopoiesis to generate mature MKs for platelet production [87]. However, our data showed that inflammation-induced emergency megakaryopoiesis more efficiently induced CXCR4^{high} MDICs than classic MKs, which further suggested the role of MKs in host-defense response.

MDICs showed phagocytosis ability and displayed efficient ability to stimulate bacterial phagocytosis ability of macrophages and neutrophils through producing TNFα and IL-6, and promoted T cell proliferation by producing IL-6. Our scRNA-seq data also showed that MDICs expressed various cytokines, such as CCL3, CCL4, CCL6 and CCL9, which regulates antimicrobial immunity [94], and IL-6, IL-15, which increases T cell proliferation and activation [80,95]. Consistently, lung MKs internalize and process both antigenic proteins and bacterial pathogens to induced CD4^{+} T cell activation in an MHC II-dependent manner [37], and exhibit transcriptomic similarity to bone marrow MDICs. Moreover, inflammation stimulates MK infiltration into the lungs. Therefore, further

studies are warranted to determine more elaborate cell surface makers and mechanisms that MDICs regulate host-defense response in various organs.

Overall, we first identified a novel immune-stimulating subpopulation, MDICs, within MKs and provided functional evidence that MDICs regulate host-defense response by enhancing the innate and adaptive immunoresponsesse.

Acknowledgments

We would like to thank the National Key Research and Development Program of China (2017YFA0103403, 2018YFA0107200), NSFC (81822001, 91749106, 81670101, 81900101, 81800164), The Key Research and Development Program of Guangdong Province (2019B020234002), Shenzhen Foundation of Science and Technology (JCYJ20170818103626421), Guangdong Innovative and Entrepreneurial Research Team Program (2016ZT06S029), Sanming Project of Medicine in Shenzhen (No.SZSM201911004), 111 Project (B13037) for generous support.

Authorship

J.W., J.X., X.H. designed and performed most of the experiments, analyzed the data and generated figures. D.W. contributed to histology and live imaging. M.C. contributed to MK ablation experiments. L.J. contributed for scientific discussion and manuscript preparation. M.Z. supervised the project and wrote the manuscript.

Conflict-of-interest disclosure

The authors declare no competing financial interests.

References

1. Notta F, Zandi S, Takayama N, et al. Distinct routes of lineage development reshape the human blood hierarchy across ontogeny. *Science*. 2016;351(6269):aab2116.
2. Deutsch VR, Tomer A. Megakaryocyte development and platelet production. *Br J Haematol*. 2006;134(5):453-466.
3. Nagata Y, Muro Y, Todokoro K. Thrombopoietin-induced polyploidization of bone marrow megakaryocytes is due to a unique regulatory mechanism in late mitosis. *J Cell Biol*. 1997;139(2):449-457.
4. Patel SR, Hartwig JH, Italiano JE, Jr. The biogenesis of platelets from megakaryocyte proplatelets. *J Clin Invest*. 2005;115(12):3348-3354.
5. Machlus KR, Italiano JE, Jr. The incredible journey: From megakaryocyte development to platelet formation. *J Cell Biol*. 2013;201(6):785-796.
6. Deutsch VR, Tomer A. Advances in megakaryocytopoiesis and thrombopoiesis: from bench to bedside. *Br J Haematol*. 2013;161(6):778-793.
7. Chang Y, Bluteau D, Debili N, Vainchenker W. From hematopoietic stem cells to platelets. *J Thromb Haemost*. 2007;5 Suppl 1:318-327.
8. Avecilla ST, Hattori K, Heissig B, et al. Chemokine-mediated interaction of hematopoietic progenitors with the bone marrow vascular niche is required for thrombopoiesis. *Nat Med*. 2004;10(1):64-71.
9. Tamura S, Suzuki-Inoue K, Tsukiji N, et al. Podoplanin-positive periarteriolar stromal cells promote megakaryocyte growth and proplatelet formation in mice by CLEC-2. *Blood*. 2016;127(13):1701-1710.
10. Pal K, Nowak R, Billington N, et al. Megakaryocyte migration defects due to nonmuscle myosin IIA mutations underlie thrombocytopenia in MYH9-related disease. *Blood*. 2020;135(21):1887-1898.
11. Wang JF, Liu ZY, Groopman JE. The alpha-chemokine receptor CXCR4 is expressed on the megakaryocytic lineage from progenitor to platelets and modulates migration and adhesion. *Blood*. 1998;92(3):756-764.
12. Lefrancais E, Ortiz-Munoz G, Caudrillier A, et al. The lung is a site of platelet biogenesis and a reservoir for haematopoietic progenitors. *Nature*. 2017;544(7648):105-+.
13. Avecilla ST, Hattori K, Heissig B, et al. Chemokine-mediated interaction of hematopoietic progenitors with the bone marrow vascular niche is required for thrombopoiesis. *Nature Medicine*. 2004;10(1):64-71.
14. Fuentes R, Wang YH, Hirsch J, et al. Infusion of mature megakaryocytes into mice yields functional platelets. *Journal of Clinical Investigation*. 2010;120(11):3917-3922.
15. Zhao M, Perry JM, Marshall H, et al. Megakaryocytes maintain homeostatic quiescence and promote post-injury regeneration of hematopoietic stem cells. *Nat Med*. 2014;20(11):1321-1326.
16. Di Giandomenico S, Kermani P, Molle N, et al. Megakaryocyte TGFbeta1 Partitions Erythropoiesis into Immature Progenitor/Stem Cells and Maturing Precursors. *Blood*. 2020.
17. Bruns I, Lucas D, Pinho S, et al. Megakaryocytes regulate hematopoietic stem cell quiescence through CXCL4 secretion. *Nat Med*. 2014;20(11):1315-1320.
18. Olson TS, Caselli A, Otsuru S, et al. Megakaryocytes promote murine osteoblastic HSC niche

expansion and stem cell engraftment after radioablative conditioning. *Blood*. 2013.
19. Dominici M, Rasini V, Bussolari R, et al. Restoration and reversible expansion of the osteoblastic hematopoietic stem cell niche after marrow radioablation. *Blood*. 2009;114(11):2333-2343.
20. Yamazaki S, Ema H, Karlsson G, et al. Nonmyelinating Schwann cells maintain hematopoietic stem cell hibernation in the bone marrow niche. *Cell*. 2011;147(5):1146-1158.
21. Jiang L, Han X, Wang J, et al. SHP-1 regulates hematopoietic stem cell quiescence by coordinating TGF-beta signaling. *J Exp Med*. 2018;215(5):1337-1347.
22. Sacma M, Pospiech J, Bogeska R, et al. Haematopoietic stem cells in perisinusoidal niches are protected from ageing. *Nat Cell Biol*. 2019;21(11):1309-1320.
23. Shiraki R, Inoue N, Kawasaki S, et al. Expression of Toll-like receptors on human platelets. *Thromb Res*. 2004;113(6):379-385.
24. Rabellino EM, Levene RB, Nachman RL, Leung LL. Human megakaryocytes. III. Characterization in myeloproliferative disorders. *Blood*. 1984;63(3):615-622.
25. Zufferey A, Speck ER, Machlus KR, et al. Mature murine megakaryocytes present antigen-MHC class I molecules to T cells and transfer them to platelets. *Blood Adv*. 2017;1(20):1773-1785.
26. Cunin P, Penke LR, Thon JN, et al. Megakaryocytes compensate for Kit insufficiency in murine arthritis. *J Clin Invest*. 2017;127(5):1714-1724.
27. Winter O, Moser K, Mohr E, et al. Megakaryocytes constitute a functional component of a plasma cell niche in the bone marrow. *Blood*. 2010;116(11):1867-1875.
28. Deuel TF, Senior RM, Chang D, Griffin GL, Heinrikson RL, Kaiser ET. Platelet factor 4 is chemotactic for neutrophils and monocytes. *Proceedings of the National Academy of Sciences*. 1981;78(7):4584.
29. Fava RA, Olsen NJ, Postlethwaite AE, et al. Transforming growth factor beta 1 (TGF-beta 1) induced neutrophil recruitment to synovial tissues: implications for TGF-beta-driven synovial inflammation and hyperplasia. *J Exp Med*. 1991;173(5):1121-1132.
30. Brandes ME, Mai UE, Ohura K, Wahl SM. Type I transforming growth factor-beta receptors on neutrophils mediate chemotaxis to transforming growth factor-beta. *J Immunol*. 1991;147(5):1600-1606.
31. Couldwell G, Machlus KR. Modulation of megakaryopoiesis and platelet production during inflammation. *Thromb Res*. 2019;179:114-120.
32. Cunin P, Nigrovic PA. Megakaryocytes as immune cells. *J Leukoc Biol*. 2019;105(6):1111-1121.
33. Gaertner F, Massberg S. Patrolling the vascular borders: platelets in immunity to infection and cancer. *Nat Rev Immunol*. 2019;19(12):747-760.
34. Semple JW, Italiano JE, Jr., Freedman J. Platelets and the immune continuum. *Nat Rev Immunol*. 2011;11(4):264-274.
35. Butler A, Hoffman P, Smibert P, Papalexi E, Satija R. Integrating single-cell transcriptomic data across different conditions, technologies, and species. *Nat Biotechnol*. 2018;36(5):411-420.
36. Yeung AK, Villacorta-Martin C, Hon S, Rock JR, Murphy GJ. Lung megakaryocytes display distinct transcriptional and phenotypic properties. *Blood Adv*. 2020;4(24):6204-6217.
37. Pariser DN, Hilt ZT, Ture SK, et al. Lung megakaryocytes are immune modulatory cells. *J Clin Invest*. 2021;131(1).

38. Xie X, Shi Q, Wu P, et al. Single-cell transcriptome profiling reveals neutrophil heterogeneity in homeostasis and infection. *Nature Immunology*. 2020;21(9):1119-1133.
39. Raslova H, Roy L, Vourc'h C, et al. Megakaryocyte polyploidization is associated with a functional gene amplification. *Blood*. 2003;101(2):541-544.
40. Noetzli LJ, French SL, Machlus KR. New Insights Into the Differentiation of Megakaryocytes From Hematopoietic Progenitors. *Arteriosclerosis Thrombosis and Vascular Biology*. 2019;39(7):1288-1300.
41. Tijssen MR, Cvejic A, Joshi A, et al. Genome-wide analysis of simultaneous GATA1/2, RUNX1, FLI1, and SCL binding in megakaryocytes identifies hematopoietic regulators. *Dev Cell*. 2011;20(5):597-609.
42. Xing Y, Zhang J, Lu L, et al. Identification of hub genes of pneumocyte senescence induced by thoracic irradiation using weighted gene coexpression network analysis. *Mol Med Rep*. 2016;13(1):107-116.
43. Lampert IA, Horncastle D, Dilworth S, Roberts I, Alison MR, Naresh KN. The expression of minichromosome maintenance protein-2 in normal and abnormal megakaryocytes and comparison with the proliferative marker Ki-67. *Br J Haematol*. 2005;131(4):490-494.
44. Raslova H, Kauffmann A, Sekkaï D, et al. Interrelation between polyploidization and megakaryocyte differentiation: a gene profiling approach. *Blood*. 2006;109(8):3225-3234.
45. Nilsen H, Rosewell I, Robins P, et al. Uracil-DNA Glycosylase (UNG)-Deficient Mice Reveal a Primary Role of the Enzyme during DNA Replication. *Molecular Cell*. 2000;5(6):1059-1065.
46. Kaur G, Jalagadugula G, Mao G, Rao AK. RUNX1/core binding factor A2 regulates platelet 12-lipoxygenase gene (ALOX12): studies in human RUNX1 haplodeficiency. *Blood*. 2010;115(15):3128-3135.
47. Kanaji S, Kanaji T, Jacquelin B, et al. Thrombopoietin initiates demethylation-based transcription of GP6 during megakaryocyte differentiation. *Blood*. 2005;105(10):3888-3892.
48. Sabri S, Jandrot-Perrus M, Bertoglio J, et al. Differential regulation of actin stress fiber assembly and proplatelet formation by α2β1 integrin and GPVI in human megakaryocytes. *Blood*. 2004;104(10):3117-3125.
49. Wang H, He J, Xu C, et al. Decoding Human Megakaryocyte Development. *Cell Stem Cell*. 2021.
50. Stables MJ, Shah S, Camon EB, et al. Transcriptomic analyses of murine resolution-phase macrophages. *Blood*. 2011;118(26):e192-208.
51. Shi GP, Villadangos JA, Dranoff G, et al. Cathepsin S required for normal MHC class II peptide loading and germinal center development. *Immunity*. 1999;10(2):197-206.
52. Nguyen KD, Fentress SJ, Qiu Y, Yun K, Cox JS, Chawla A. Circadian gene Bmal1 regulates diurnal oscillations of Ly6C(hi) inflammatory monocytes. *Science*. 2013;341(6153):1483-1488.
53. Li ZH, Dulyaninova NG, House RP, Almo SC, Bresnick AR. S100A4 regulates macrophage chemotaxis. *Mol Biol Cell*. 2010;21(15):2598-2610.
54. Zhou T, Damsky W, Weizman OE, et al. IL-18BP is a secreted immune checkpoint and barrier to IL-18 immunotherapy. *Nature*. 2020;583(7817):609-614.
55. Thomsen MK, Bakiri L, Hasenfuss SC, Hamacher R, Martinez L, Wagner EF. JUNB/AP-1 controls IFN-gamma during inflammatory liver disease. *J Clin Invest*. 2013;123(12):5258-5268.

56. Tanaka T, Narazaki M, Kishimoto T. IL-6 in inflammation, immunity, and disease. *Cold Spring Harb Perspect Biol*. 2014;6(10):a016295.
57. Mocsai A, Humphrey MB, Van Ziffle JA, et al. The immunomodulatory adapter proteins DAP12 and Fc receptor gamma-chain (FcRgamma) regulate development of functional osteoclasts through the Syk tyrosine kinase. *Proc Natl Acad Sci U S A*. 2004;101(16):6158-6163.
58. Li S, Qin X, Chai S, Qu C, Wang X, Zhang H. Modulation of E-cadherin expression promotes migration ability of esophageal cancer cells. *Sci Rep*. 2016;6:21713.
59. Kojima T, Obata K, Mukai K, et al. Mast cells and basophils are selectively activated in vitro and in vivo through CD200R3 in an IgE-independent manner. *J Immunol*. 2007;179(10):7093-7100.
60. Hsu HJ, Liang MR, Chen CT, Chung BC. Pregnenolone stabilizes microtubules and promotes zebrafish embryonic cell movement. *Nature*. 2006;439(7075):480-483.
61. Hirano T, Koyanagi A, Kotoshiba K, et al. The Fab fragment of anti-IgE Cepsilon2 domain prevents allergic reactions through interacting with IgE-FcepsilonRIalpha complex on rat mast cells. *Sci Rep*. 2018;8(1):14237.
62. Cheng SS, Lai JJ, Lukacs NW, Kunkel SL. Granulocyte-macrophage colony stimulating factor up-regulates CCR1 in human neutrophils. *J Immunol*. 2001;166(2):1178-1184.
63. Arlt A, Schafer H. Role of the immediate early response 3 (IER3) gene in cellular stress response, inflammation and tumorigenesis. *Eur J Cell Biol*. 2011;90(6-7):545-552.
64. Scott EW, Fisher RC, Olson MC, Kehrli EW, Simon MC, Singh H. PU.1 functions in a cell-autonomous manner to control the differentiation of multipotential lymphoid-myeloid progenitors. *Immunity*. 1997;6(4):437-447.
65. Hirata Y, Furuhashi K, Ishii H, et al. CD150(high) Bone Marrow Tregs Maintain Hematopoietic Stem Cell Quiescence and Immune Privilege via Adenosine. *Cell Stem Cell*. 2018;22(3):445-453 e445.
66. Gazit R, Mandal PK, Ebina W, et al. Fgd5 identifies hematopoietic stem cells in the murine bone marrow. *J Exp Med*. 2014;211(7):1315-1331.
67. Iwasaki H, Arai F, Kubota Y, Dahl M, Suda T. Endothelial protein C receptor-expressing hematopoietic stem cells reside in the perisinusoidal niche in fetal liver. *Blood*. 2010;116(4):544-553.
68. Chen JY, Miyanishi M, Wang SK, et al. Hoxb5 marks long-term haematopoietic stem cells and reveals a homogenous perivascular niche. *Nature*. 2016;530(7589):223-227.
69. Wang J-F, Liu Z-Y, Groopman JE. The α-Chemokine Receptor CXCR4 Is Expressed on the Megakaryocytic Lineage From Progenitor to Platelets and Modulates Migration and Adhesion. *Blood*. 1998;92(3):756-764.
70. Suraneni PK, Corey SJ, Hession MJ, et al. Dynamins 2 and 3 control the migration of human megakaryocytes by regulating CXCR4 surface expression and ITGB1 activity. *Blood Adv*. 2018;2(23):3540-3552.
71. Ng AP, Kauppi M, Metcalf D, et al. Mpl expression on megakaryocytes and platelets is dispensable for thrombopoiesis but essential to prevent myeloproliferation. *Proc Natl Acad Sci U S A*. 2014;111(16):5884-5889.
72. Takizawa H, Fritsch K, Kovtonyuk LV, et al. Pathogen-Induced TLR4-TRIF Innate Immune Signaling in Hematopoietic Stem Cells Promotes Proliferation but Reduces Competitive Fitness. *Cell Stem Cell*.

2017;21(2):225-240 e225.
73. Itkin T, Gur-Cohen S, Spencer JA, et al. Distinct bone marrow blood vessels differentially regulate haematopoiesis. *Nature*. 2016;532(7599):323-328.
74. Tiedt R, Schomber T, Hao-Shen H, Skoda RC. Pf4-Cre transgenic mice allow the generation of lineage-restricted gene knockouts for studying megakaryocyte and platelet function in vivo. *Blood*. 2007;109(4):1503-1506.
75. Edelson BT, Unanue ER. Immunity to Listeria infection. *Curr Opin Immunol*. 2000;12(4):425-431.
76. Conlan JW. Early host-pathogen interactions in the liver and spleen during systemic murine listeriosis: an overview. *Immunobiology*. 1999;201(2):178-187.
77. Bruns I, Lucas D, Pinho S, et al. Megakaryocytes regulate hematopoietic stem cell quiescence through CXCL4 secretion. *Nat Med*. 2014;20(11):1315-1320.
78. Rothe G, Kellermann W, Briegel J, Schaerer B, Valet G. Activation of Neutrophils by Tumor Necrosis Factor-α During Sepsis. In: Faist E, Meakins JL, Schildberg FW, eds. Host Defense Dysfunction in Trauma, Shock and Sepsis: Mechanisms and Therapeutic Approaches. Berlin, Heidelberg: Springer Berlin Heidelberg; 1993:727-735.
79. Shapouri-Moghaddam A, Mohammadian S, Vazini H, et al. Macrophage plasticity, polarization, and function in health and disease. *J Cell Physiol*. 2018;233(9):6425-6440.
80. Li B, Jones LL, Geiger TL. IL-6 Promotes T Cell Proliferation and Expansion under Inflammatory Conditions in Association with Low-Level RORγt Expression. *Journal of immunology (Baltimore, Md : 1950)*. 2018;201(10):2934-2946.
81. Kotsias F, Cebrian I, Alloatti A. Chapter Two - Antigen processing and presentation. In: Lhuillier C, Galluzzi L, eds. International Review of Cell and Molecular Biology. Vol. 348: Academic Press; 2019:69-121.
82. Cheon H, Holvey-Bates EG, Schoggins JW, et al. IFNβ-dependent increases in STAT1, STAT2, and IRF9 mediate resistance to viruses and DNA damage. *The EMBO Journal*. 2013;32(20):2751-2763.
83. MacMicking JD. Interferon-inducible effector mechanisms in cell-autonomous immunity. *Nature Reviews Immunology*. 2012;12(5):367-382.
84. Spence JS, He R, Hoffmann H-H, et al. IFITM3 directly engages and shuttles incoming virus particles to lysosomes. *Nature Chemical Biology*. 2019;15(3):259-268.
85. Verschoor A, Neuenhahn M, Navarini AA, et al. A platelet-mediated system for shuttling blood-borne bacteria to CD8 alpha(+) dendritic cells depends on glycoprotein GPIb and complement C3. *Nature Immunology*. 2011;12(12):1194-U1186.
86. Nishimura S, Nagasaki M, Kunishima S, et al. IL-1α induces thrombopoiesis through megakaryocyte rupture in response to acute platelet needs. *Journal of Cell Biology*. 2015;209(3):453-466.
87. Haas S, Hansson J, Klimmeck D, et al. Inflammation-Induced Emergency Megakaryopoiesis Driven by Hematopoietic Stem Cell-like Megakaryocyte Progenitors. *Cell Stem Cell*. 2015;17(4):422-434.
88. Beaulieu LM, Lin E, Mick E, et al. Interleukin 1 receptor 1 and interleukin 1β regulate megakaryocyte maturation, platelet activation, and transcript profile during inflammation in mice and humans. *Arteriosclerosis, thrombosis, and vascular biology*. 2014;34(3):552-564.
89. Yang M, Li K, Chui CM, et al. Expression of interleukin (IL) 1 type I and type II receptors in

megakaryocytic cells and enhancing effects of IL-1beta on megakaryocytopoiesis and NF-E2 expression. *Br J Haematol*. 2000;111(1):371-380.

90. Beaulieu LM, Lin E, Morin KM, Tanriverdi K, Freedman JE. Regulatory effects of TLR2 on megakaryocytic cell function. *Blood*. 2011;117(22):5963-5974.

91. Campbell RA, Schwertz H, Hottz ED, et al. Human megakaryocytes possess intrinsic antiviral immunity through regulated induction of IFITM3. *Blood*. 2019;133(19):2013-2026.

92. Wang H, He J, Xu C, et al. Decoding Human Megakaryocyte Development. *Cell Stem Cell*. 2020.

93. Davis RE, Stenberg PE, Levin J, Beckstead JH. Localization of megakaryocytes in normal mice and following administration of platelet antiserum, 5-fluorouracil, or radiostrontium: evidence for the site of platelet production. *Exp Hematol*. 1997;25(7):638-648.

94. Sokol CL, Luster AD. The chemokine system in innate immunity. *Cold Spring Harb Perspect Biol*. 2015;7(5).

95. Cornish GH, Sinclair LV, Cantrell DA. Differential regulation of T-cell growth by IL-2 and IL-15. *Blood*. 2006;108(2):600-608.

Figure legends

Figure 1. Single-cell atlas identifies an MK derived inflammatory cell population. (A) Schematic depicting the strategy of cell isolation, MK sorting, scRNA-seq and data analysis. (B) UMAP of 1,712 MKs from bone marrow, colored by clusters. (C) Violin plots showing the expression of MK selected marker genes. (D) Feature plots of MK marker genes. (E) Heat map showing the row-scaled signature genes of MKs (fold-change > 1.5, p value < 0.05) with exemplar genes listed on the right (top, color-coded by clusters). Columns denote cells; rows denote genes. (F) Dot plot showing the scaled expression of exemplar signature genes for each cluster, colored by the average expression of each gene in each cluster scaled across all clusters. Dot size represents the percentage of expressed cells in each cluster. (G) Feature plots of selected signature genes in each cluster. (H) Gene Ontology (GO) analysis of signature genes for each cluster. GO terms are selected with Benjamini–Hochberg-corrected p values < 0.05 and colored by $-\log_{10}(p \text{ value})$. (I) Violin plots and the corresponding feature plots of selected signature genes of MK5.

Figure 2. MDICs migrate to peripheral organs upon *L. monocytogenes* infection. (A) Schematic depicting the strategy of *L. monocytogenes* infection and analysis. (B-D) Bone marrow MK (B), CXCR4^{low} MK (C) and CXCR4^{high} MK (D) numbers of control mice and mice at three days after *L. monocytogenes* infection (n = 8 mice). (E-F) Fraction of CXCR4^{high} BrdU^{+} MKs (E) and CXCR4^{high}Annexin V^{+} MKs (F) in bone marrow from control mice or mice at three days after *L. monocytogenes* infection (n = 5 mice). (G) GSEA evaluated enrichment of chemotaxis and cell migration genes in MK5 cells compared to classic MK populations (MK1 to 4). Normalized enrichment scores (NESs)

and adjusted *p* values were calculated by permutation tests. (H) Representative images of CD41 (blue), CD150 (red), EMCN (green) and lineage cells (white) in bone marrow from control mice or mice at three days after *L. monocytogenes* infection. d_{HSC} and d_{EC} indicate the distance between the MK (blue, marked with an asterisk) and the closest HSC (red), endothelia cell (green), respectively. Yellow boxes indicate the locations of the magnified images. Arrowheads indicate HSCs. EMCN, endomucin; EC, endothelial cell. (I-J) Comparison of distance between HSCs to MKs (n = 96 control and 127 infected HSCs, p = 0.21 by two-sample KS test) (I), and MKs to ECs (n = 119 control and 103 infected MKs) (J) in bone marrow of control mice or mice at three days after *L. monocytogenes* infection. (K) Representative images of CD41 (blue), CXCR4 (red) and EMCN (green) in bone marrow of mice at three days after *L. monocytogenes* infection. Yellow arrows indicate $CXCR4^{high}$ MKs, while white arrowheads indicate $CXCR4^{low}$ MKs. (L) Comparison of distance between $CXCR4^{low}$ or $CXCR4^{high}$ MKs and ECs (n = 68 $CXCR4^{low}$ and 78 $CXCR4^{high}$ MKs). (M) Visualization of MK migration (red, arrowhead) into the BM sinusoids (green) by live imaging in *Pf4-cre*; *tdTomato*$^{+/-}$ mice at three days after *L. monocytogenes* infection. S, indicates sinusoid and dashed lines demarcate the border of sinusoids. (N-P) $CXCR4^{high}$ MKs in peripheral blood (N), livers (O) and spleens (P) from control mice or mice at three days after *L. monocytogenes* infection (n = 3 mice). (Q-R) Representative images and cell numbers of *mGFP*$^{+}$ cells (green) in livers (Q) and spleens (R) from control mice or mice at three days after *L. monocytogenes* infection (n = 4 mice). Scale bars without indicated, 20 μm. Data represent mean ± s.e.m. Two-tailed Student's *t*-test was performed to assess statistical significance in (B-F, J, L,

N-R). * p <0.05, ** p <0.01, *** p < 0.001, n.s., no significant difference. Two-sample KS test was performed to assess statistically significant in (I).

Figure 3. MDICs promote myeloid cell migration upon *L. monocytogenes* infection. (A) GSEA evaluated enrichment of cell-cell adhesion and myeloid cell activation genes in MK5 cells compared to classic MK populations (MK1 to 4). NESs and adjusted p values were calculated by permutation tests. (B) Schematic depicting transwell assay for myeloid cells in absence or presence of MKs as indicated. (C-D) Numbers of indicated transmigrated cells, normalized to Ctrl (only media was added to the lower chambers). Mon, monocytes; MΦ, macrophages; DC, dendritic cells; Neu, neutrophils. (E) Representative images of MKs (blue), vascular endothelial cells (green) and myeloid cells (white) in mouse bone marrow. Arrowheads indicate the myeloid cells in the sinusoids. d_{MK} and d_{EC} indicate the distance between the myeloid cell marked with an asterisk to the closest MK and endothelial cell (EC), respectively. (F) Number of MKs and myeloid cells in the sinusoids of control mice or mice at three days after *L. monocytogenes* infection (n = 3 mice). (G) Two-dimensional probability distribution of distances from myeloid cells to MKs (d_{MK}) and EC cells (d_{EC}) in bone marrow of control mice or mice at three days after *L. monocytogenes* infection (control, n = 119 $CD11b^+$ cells; infection, n = 144 $CD11b^+$ cells; $p = 3 \times 10^{-5}$ by 2D KS test). (H) Representative images of MKs (blue), CXCR4 (red), vascular endothelial cells (green) and myeloid cells (white) in mouse bone marrow showing the distribution of myeloid cells to $CXCR4^{low}$ or $CXCR4^{high}$ MKs and vascular cells at three days after *L. monocytogenes* infection. Yellow arrows indicate $CXCR4^{high}$ MKs and white arrowheads indicate $CXCR4^{low}$ MKs. (I-J) Distance (I) and mean distance ($p = 7 \times 10^{-4}$ by KS test, J) of myeloid cells to the closest

CXCR4^{low} and CXR4^{high} MKs. (K) Two-dimensional probability distribution of distances from myeloid cells to CXCR4^{low} or CXCR4^{high} MKs and vascular cells (n = 104 CD11b^{+} cells; p = 0.04 by 2D KS test). (L) Schema for DT treatment and *L. monocytogenes* infection design. *L.m.*, *L. monocytogenes*. (M) Representative images of MKs (blue, arrows) and vascular endothelial cells (green) in bone marrow of mice after 4 days diphtheria toxin (DT) treatment. (N-P) Percentage or cell number of innate immune cells in bone marrow (N), livers (O) or spleens (P) of *Pf4-cre*; *iDTR*$^{+/-}$ mice after four-time DT injections (n = 6 mice). Scale bars, 20 μm. Data represent mean ± s.e.m. Repeated-measures one-way ANOVA followed by Dunnett's test for multiple comparisons in (C-D), ♮ p <0.05, ♯ p <0.01, ♯♯ p <0.001, n.s., no significant difference. Two-dimensional-two-sample KS test was performed to assess statistically significant in (G, K). Two-sample KS test was performed to assess statistically significant in (J). Two-tailed Student's t-test was performed to assess statistical significance in (F, N-P). * p <0.05, ** p <0.01, *** p <0.001, n.s., no significant difference.

Figure 4. MDICs enhance host-defense response against *L. monocytogenes* infection. (A) Representative images of neutrophil phagocytosis capacity with or without CXCR4^{low} MKs or CXCR4^{high} MKs co-cultured. CD11b, red; *E coli*, green; DAPI, blue. (B) Quantification of neutrophil phagocytosis capacity with indicated MKs co-cultured. Blank, neutrophil phagocyted without co-cultured cells (Blank, n = 20; CXCR4^{low} MKs, n = 19; CXCR4^{high} MKs, n = 20; CD324^{+} MKs, n = 23; CCR2^{+} MKs, n = 19; CCR2^{+}CXCR4^{high} MKs, n = 18). (C) Representative images of macrophage phagocytosis capacity with or without CXCR4^{low} MKs or CXCR4^{high} MKs co-cultured. F4/80, red; *E coli*, green; DAPI, blue. (D) Quantification of macrophage phagocytosis capacity with

indicated MKs co-cultured. Blank, macrophage phagocyted without co-cultured cells (Blank, n = 110; CXCR4^{low} MKs, n = 69; CXCR4^{high} MKs, n = 94; CD324^{+} MKs, n = 40; CCR2^{+} MKs, n = 184; CCR2^{+}CXCR4^{high} MKs, n = 66). (E) GSEA evaluated enrichment of cytokine production involved in immune response genes in MK5 cells compared to classic MK populations (MK1 to 4). NES and adjusted p value were calculated by permutation tests. (F) Correlation analysis between expression profiles of *Cxcr4* and cytokines, feature genes of MK subpopulations. (G-J) TNFα and IL-6 protein levels in CXCR4^{low} and CXCR4^{high} MKs were shown by FACS (G, I) and immunostaining using sorted MKs comparing to their functional levels of macrophages (H, J). (K-L) Quantification of neutrophil (K) and macrophage (L) phagocytosis capacity with or without CXCR4^{high} MKs co-cultured in absence or presence of TNFα neutralizing antibody (neutrophil: n = 30 for each group; macrophage: Blank, n = 36; CXCR4^{high} MKs, n = 34; CXCR4^{high} MKs + TNFα neutralizing antibody, n = 34). Blank, neutrophil phagocyted without co-cultured cells. (M-N) Quantification of neutrophil (M) and macrophage (N) phagocytosis capacity with or without CXCR4^{high} MKs co-cultured in absence or presence of IL-6 neutralizing antibody (neutrophil: Blank, n = 20; CXCR4^{high} MKs, n = 20; CXCR4^{high} MKs + IL-6 neutralizing antibody, n = 19; macrophage: Blank, n = 44; CXCR4^{high} MKs, n = 36; CXCR4^{high} MKs + IL-6 neutralizing antibody, n = 39). (O) Schema for DT treatment and *L. monocytogenes* infection. (P-Q) Numbers of *L. monocytogenes* CFUs of livers (P) and spleens (Q) of *Pf4-cre*; *iDTR*$^{+}$ mice at three days after *L. monocytogenes* infection (n = 6 mice). Scale bars in (A, C), 20 μm; scale bars in (H, J), 5 μm. Data represent means ± first and third quartiles (B, D, H, J-N) or mean ± s.e.m (G, I, P, Q). Two-sample KS test was performed to assess statistically significant in

(B, D, H, J-N). Two-tailed Student's *t*-test was performed to assess statistical significance in (G, I, P, Q), * p <0.05, ** p <0.01, *** p <0.001, n.s., no significant difference.

Figure 5. Bacterial infection promotes coagulation and immune response in distinct MK subpopulations. (A) Schematic depicting the strategy of scRNA-seq using bone marrow MKs from mice at three days after *L. monocytogenes* infection. (B) UMAP of 5,368 cells from control bone marrow and 4,276 cells from *L. monocytogenes* infection bone marrow, colored by cell types. Neu, neutrophil; MP, myeloid progenitor; Mon, monocytes; B, B cells; T, T cells. (C) GO analysis of up-regulated genes after *L. monocytogenes* infection (fold-change > 1.5, $p < 0.05$) for each cell types. GO terms are selected with Benjamini–Hochberg-corrected p values < 0.05 and colored by $-\log_{10}(p$ value), dot size represents the gene ratio. (D) UMAP of 3,272 MKs from control (1,712 MKs) and *L. monocytogenes* infection (1,560 MKs) bone marrow, colored by clusters. (E) Fraction of each MK cluster from control MKs or *L. monocytogenes* infection MKs. (F) Gene set variation analysis (GSVA) of each MK cluster under control or *L. monocytogenes* infection, colored by row-scaled GSVA enrichment scores. (G) Heat map showing the row-scaled differential genes of control and infection MK5 cells (fold-change > 1.4, p value < 0.05), with exemplar genes listed on the right (top, color-coded by conditions). Columns denote cells; rows denote genes. (H) Similarities by MetaNeighbor R package of scRNA-seq defined MK populations in control and *L. monocytogenes* infection BM with the BM MK and lung MK reported by Pariser et al [37] and Yeung et al [36]. (I) Heat map showing the row-scaled antigen processing genes of control and infection MK5 cells, comparing with BM MK and lung MK reported by Yeung et al [36].

Figure 6. Bacterial infection stimulates thrombopoiesis and T cell proliferation via MKs. (A-B) Representative images (A) and statistical analysis (B) of CD41 (green) and DAPI (blue) in bone marrow from control mice or mice at three days after *L. monocytogenes* infection. Arrows indicate ruptured MKs, yellow boxes indicate the locations of the magnified images. (C) Platelets in peripheral blood in control mice or mice after *L. monocytogenes* infection on indicated days. (D) Representative flow cytometry gating and the cell numbers of proliferating T cells with CXCR4^{high} MK co-cultured for 24 and 72 hours. (E) Reduced CFSE intensity of proliferating T cells with CXCR4^{low} or CXCR4^{high} MK co-cultured for 72 hours in absence or presence of IL-6 neutralizing antibody. Blank indicates T cells proliferated without co-cultured cells. (F) Schema for DT treatment, *L. monocytogenes*-OVA$_{257-264}$ infection and *in vitro* re-activation assay. *L.m.*-OVA, *L. monocytogenes*-OVA$_{257-264}$; OVA, OVA$_{257-264}$. (G) Activated T cell numbers in spleens of *Pf4-cre*; *iDTR*$^{+}$ mice after *in vitro* re-activation at seven days after *L. monocytogenes*-OVA$_{257-264}$ infection (n = 4 mice). (H) Schema for *L. monocytogenes* infection and *Pf4-cre*$^{+}$; *tdTomato*$^{+}$ cells transplantation. (I-J) Representative images and statistical analysis of lungs in control recipients or upon *L. monocytogenes* infection (n = 3 mice). Arrows indicate tdTomato^{+} cells in lungs. (K) Schema for HSC lineage tracing upon *L. monocytogenes* infection using *Scl-cre*$^{+}$; *tdTomato*$^{+/-}$ mice. (L) tdTomato^{+} CXCR4^{low} and tdTomato^{+} CXCR4^{high} MK numbers in control and *L. monocytogenes* infected *Scl-cre*$^{+}$; *tdTomato*$^{+/-}$ mice. (M) tdTomato^{+} progenitors in control and *L. monocytogenes* infected *Scl-cre*$^{+}$; *tdTomato*$^{+/-}$ mice, CMP, common myeloid progenitors; GMP, granulocyte-monocyte progenitors; MEP, megakaryocyte-erythroid progenitors. Scale bars, 20 μm. Data represent mean ± s.e.m (B,

C, E, G, J, L, M). Two-tailed Student's *t*-test was performed to assess statistical significance, * $p < 0.05$, ** $p < 0.01$, *** $p < 0.001$, n.s., no significant difference.

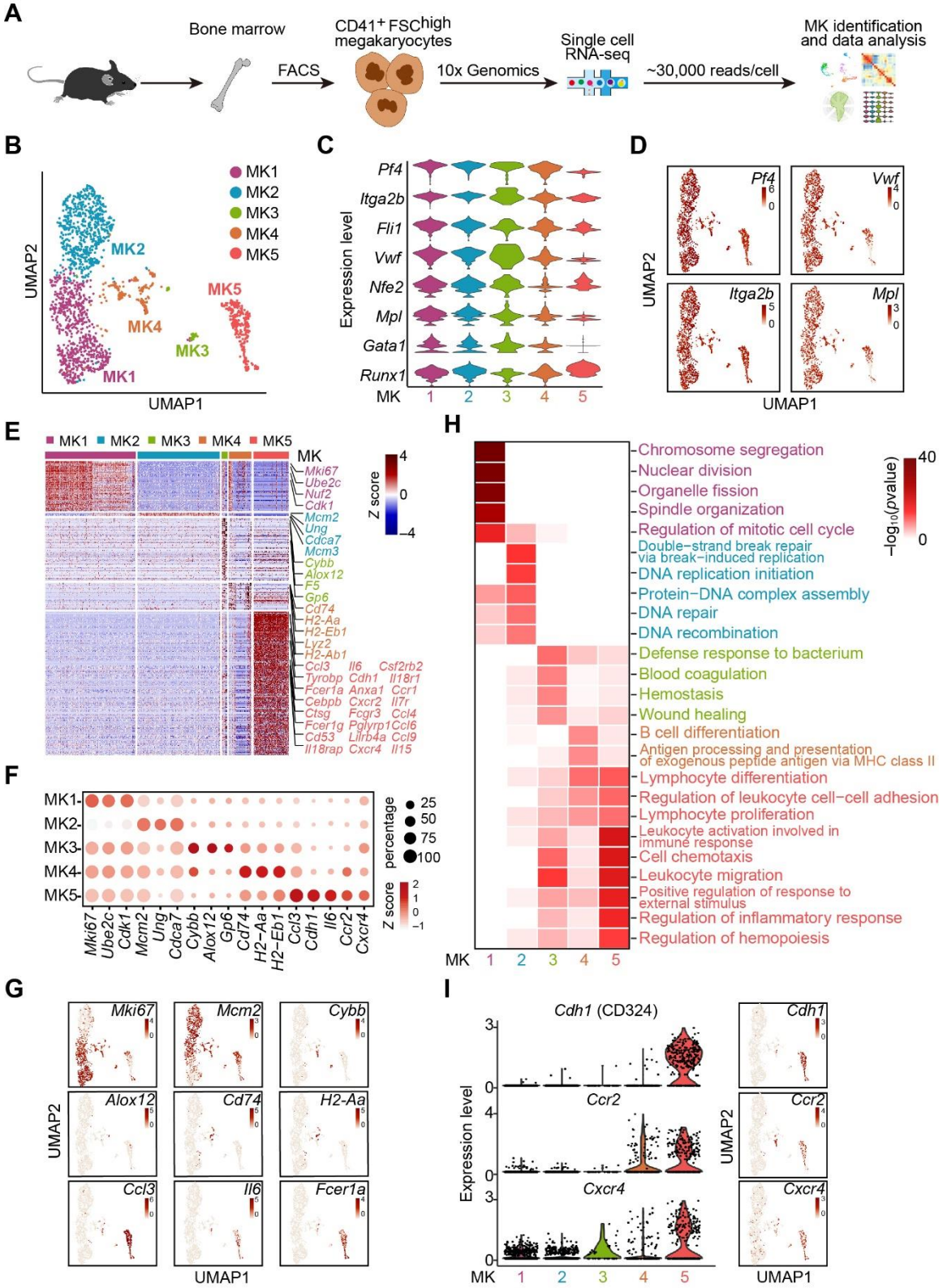
A
Bone marrow
FACS
CD41+ FSChigh megakaryocytes
10x Genomics
Single cell RNA-seq
~30,000 reads/cell
MK identification and data analysis
B
MK1
MK2
MK3
MK4
MK5
UMAP2
UMAP1
C
Pf4
Itga2b
Fli1
Vwf
Nfe2
Mpl
Gata1
Runx1
Expression level
MK
D
Pf4
Vwf
Itga2b
Mpl
UMAP2
UMAP1
E
MK1 MK2 MK3 MK4 MK5
MK
Mki67
Ube2c
Nuf2
Cdk1
Mcm2
Ung
Cdca7
Mcm3
Cybb
Alox12
F5
Gp6
Cd74
H2-Aa
H2-Eb1
Lyz2
H2-Ab1
Ccl3 Il6 Csf2rb2
Tyrobp Cdh1 Il18r1
Fcer1a Anxa1 Ccr1
Cebpb Cxcr2 Il7r
Ctsg Fcgr3 Ccl4
Fcer1g Pglyrp1 Ccl6
Cd53 Lilrb4a Ccl9
Il18rap Cxcr4 Il15
Z score
F
MK1
MK2
MK3
MK4
MK5
Mki67
Ube2c
Cdk1
Mcm2
Ung
Cdca7
Cybb
Alox12
Gp6
Cd74
H2-Aa
H2-Eb1
Ccl3
Cdh1
Il6
Ccr2
Cxcr4
percentage
Z score
H
Chromosome segregation
Nuclear division
Organelle fission
Spindle organization
Regulation of mitotic cell cycle
Double-strand break repair via break-induced replication
DNA replication initiation
Protein-DNA complex assembly
DNA repair
DNA recombination
Defense response to bacterium
Blood coagulation
Hemostasis
Wound healing
B cell differentiation
Antigen processing and presentation of exogenous peptide antigen via MHC class II
Lymphocyte differentiation
Regulation of leukocyte cell-cell adhesion
Lymphocyte proliferation
Leukocyte activation involved in immune response
Cell chemotaxis
Leukocyte migration
Positive regulation of response to external stimulus
Regulation of inflammatory response
Regulation of hemopoiesis
−log10(pvalue)
MK
G
Mki67
Mcm2
Cybb
Alox12
Cd74
H2-Aa
Ccl3
Il6
Fcer1a
UMAP2
UMAP1
I
Cdh1 (CD324)
Ccr2
Cxcr4
Expression level
MK
Cdh1
Ccr2
Cxcr4
UMAP2
UMAP1

Figure 1

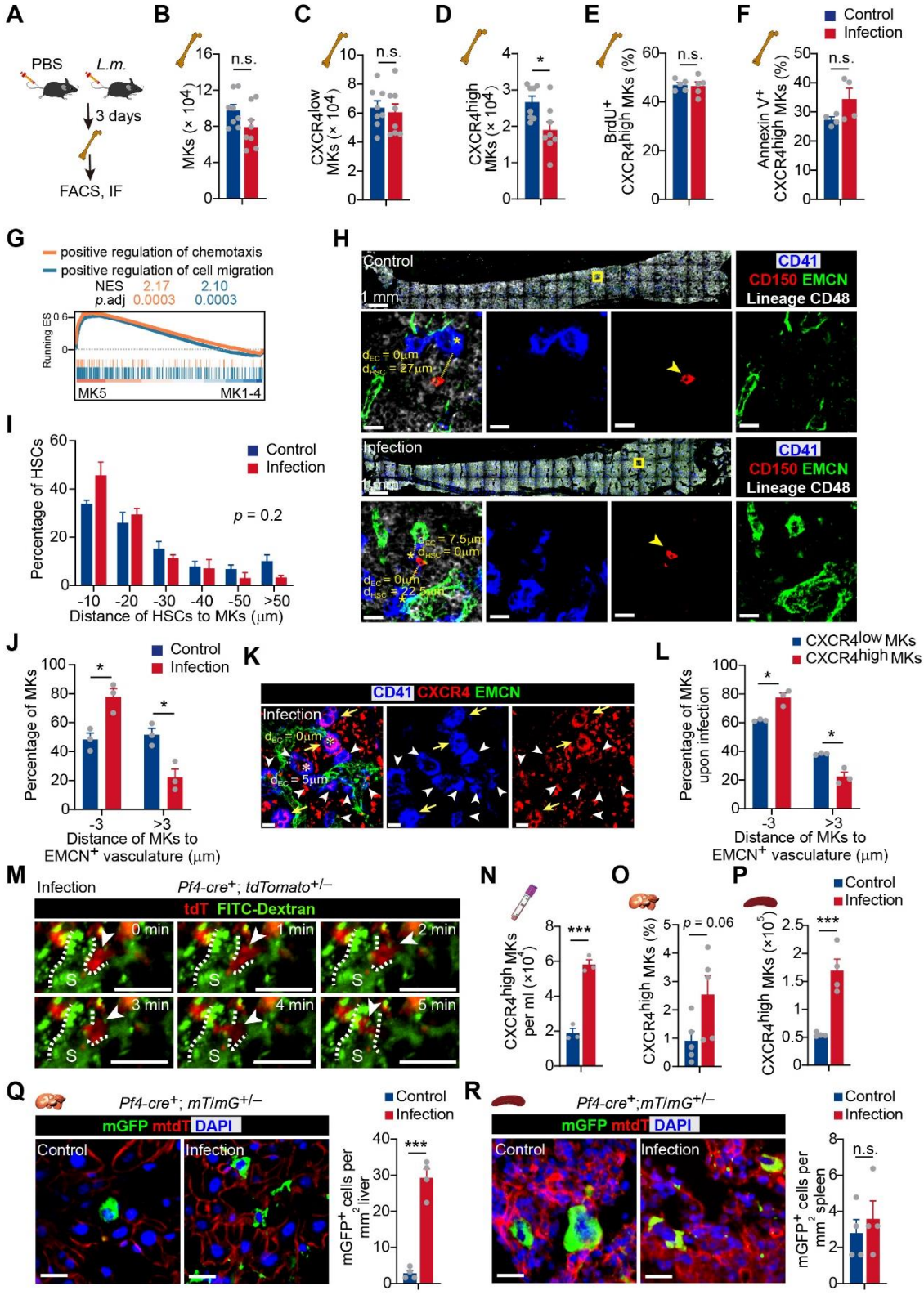
A
PBS
L.m.
3 days
FACS, IF
B
MKs (× 10⁴)
n.s.
C
CXCR4low MKs (× 10⁴)
n.s.
D
CXCR4high MKs (× 10⁴)
*
E
BrdU+ CXCR4high MKs (%)
n.s.
F
Control
Infection
Annexin V+ CXCR4high MKs (%)
n.s.
G
positive regulation of chemotaxis
positive regulation of cell migration
NES 2.17 2.10
p.adj 0.0003 0.0003
Running ES
MK5
MK1-4
H
Control
1 mm
CD41
CD150 EMCN
Lineage CD48
Infection
I
Percentage of HSCs
Control
Infection
p = 0.2
Distance of HSCs to MKs (μm)
J
Percentage of MKs
Control
Infection
Distance of MKs to EMCN+ vasculature (μm)
K
CD41 CXCR4 EMCN
Infection
L
CXCR4low MKs
CXCR4high MKs
Percentage of MKs upon infection
Distance of MKs to EMCN+ vasculature (μm)
M
Infection
Pf4-cre+; tdTomato+/–
tdT FITC-Dextran
0 min
1 min
2 min
3 min
4 min
5 min
N
CXCR4high MKs per ml (×10⁴)
***
O
CXCR4high MKs (%)
p = 0.06
P
CXCR4high MKs (×10⁵)
***
Q
Pf4-cre+; mTmG+/–
mGFP mtdT DAPI
Control
Infection
mGFP+ cells per mm² liver
***
R
Pf4-cre+;mTmG+/–
mGFP mtdT DAPI
Control
Infection
mGFP+ cells per mm² spleen
n.s.

Figure 2

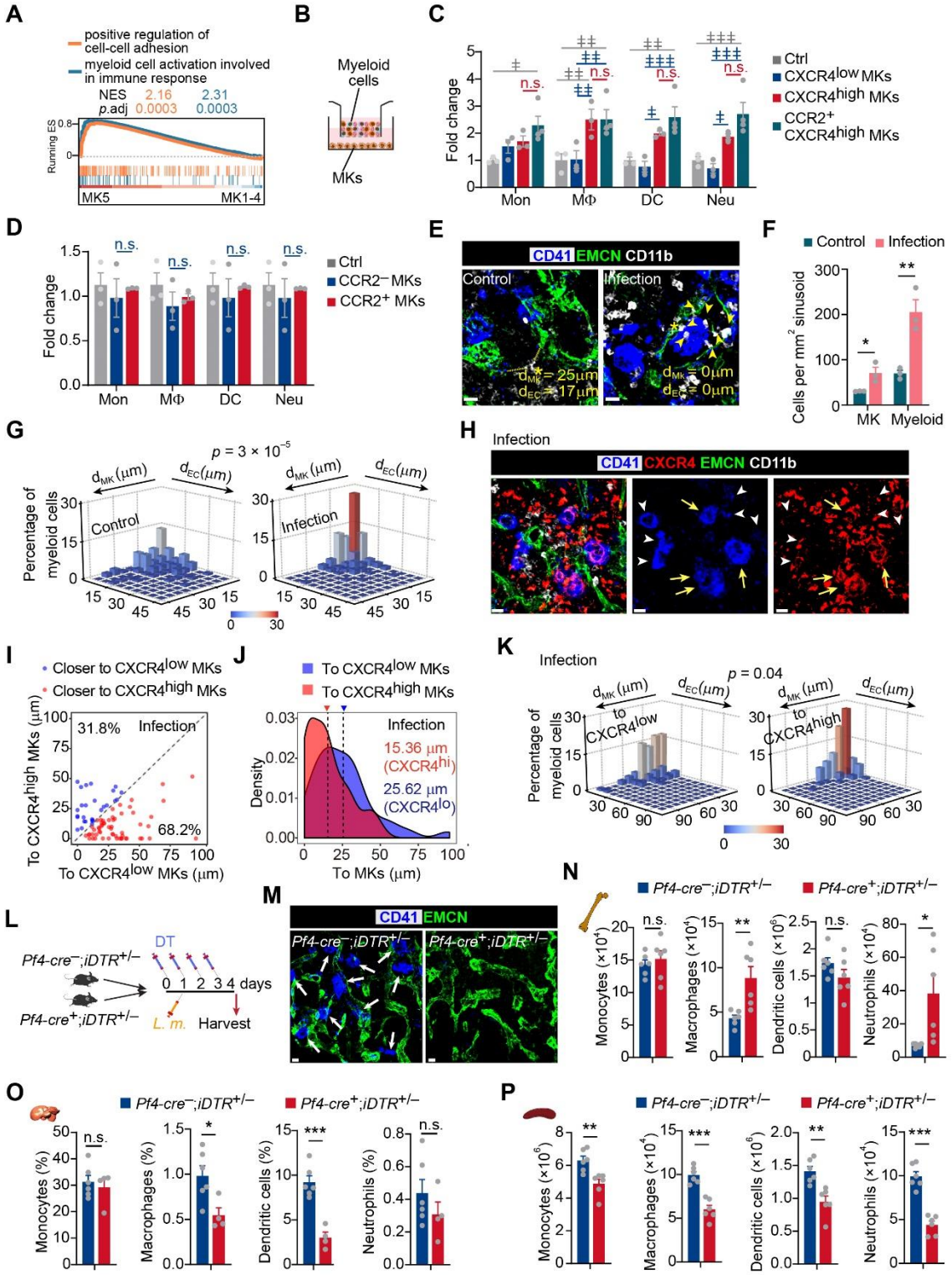
A
positive regulation of cell-cell adhesion
myeloid cell activation involved in immune response
NES 2.16 2.31
p.adj 0.0003 0.0003
Running ES
MK5
MK1-4
B
Myeloid cells
MKs
C
Fold change
Ctrl
CXCR4low MKs
CXCR4high MKs
CCR2+ CXCR4high MKs
Mon
MΦ
DC
Neu
n.s.
D
Fold change
Ctrl
CCR2− MKs
CCR2+ MKs
E
CD41 EMCN CD11b
Control
Infection
F
Control
Infection
Cells per mm2 sinusoid
MK
Myeloid
G
p = 3 × 10−5
dMK (μm)
dEC (μm)
Percentage of myeloid cells
Control
Infection
H
Infection
CD41 CXCR4 EMCN CD11b
I
Closer to CXCR4low MKs
Closer to CXCR4high MKs
31.8%
68.2%
Infection
To CXCR4high MKs (μm)
To CXCR4low MKs (μm)
J
To CXCR4low MKs
To CXCR4high MKs
Infection
15.36 μm (CXCR4hi)
25.62 μm (CXCR4lo)
Density
To MKs (μm)
K
Infection
p = 0.04
to CXCR4low
to CXCR4high
Percentage of myeloid cells
L
Pf4-cre−;iDTR+/−
Pf4-cre+;iDTR+/−
DT
0 1 2 3 4 days
L. m.
Harvest
M
CD41 EMCN
Pf4-cre−;iDTR+/−
Pf4-cre+;iDTR+/−
N
Monocytes (×10^4)
Macrophages (×10^4)
Dendritic cells (×10^6)
Neutrophils (×10^4)
O
Monocytes (%)
Macrophages (%)
Dendritic cells (%)
Neutrophils (%)
P
Monocytes (×10^6)
Macrophages (×10^4)
Dendritic cells (×10^6)
Neutrophils (×10^4)

Figure 3

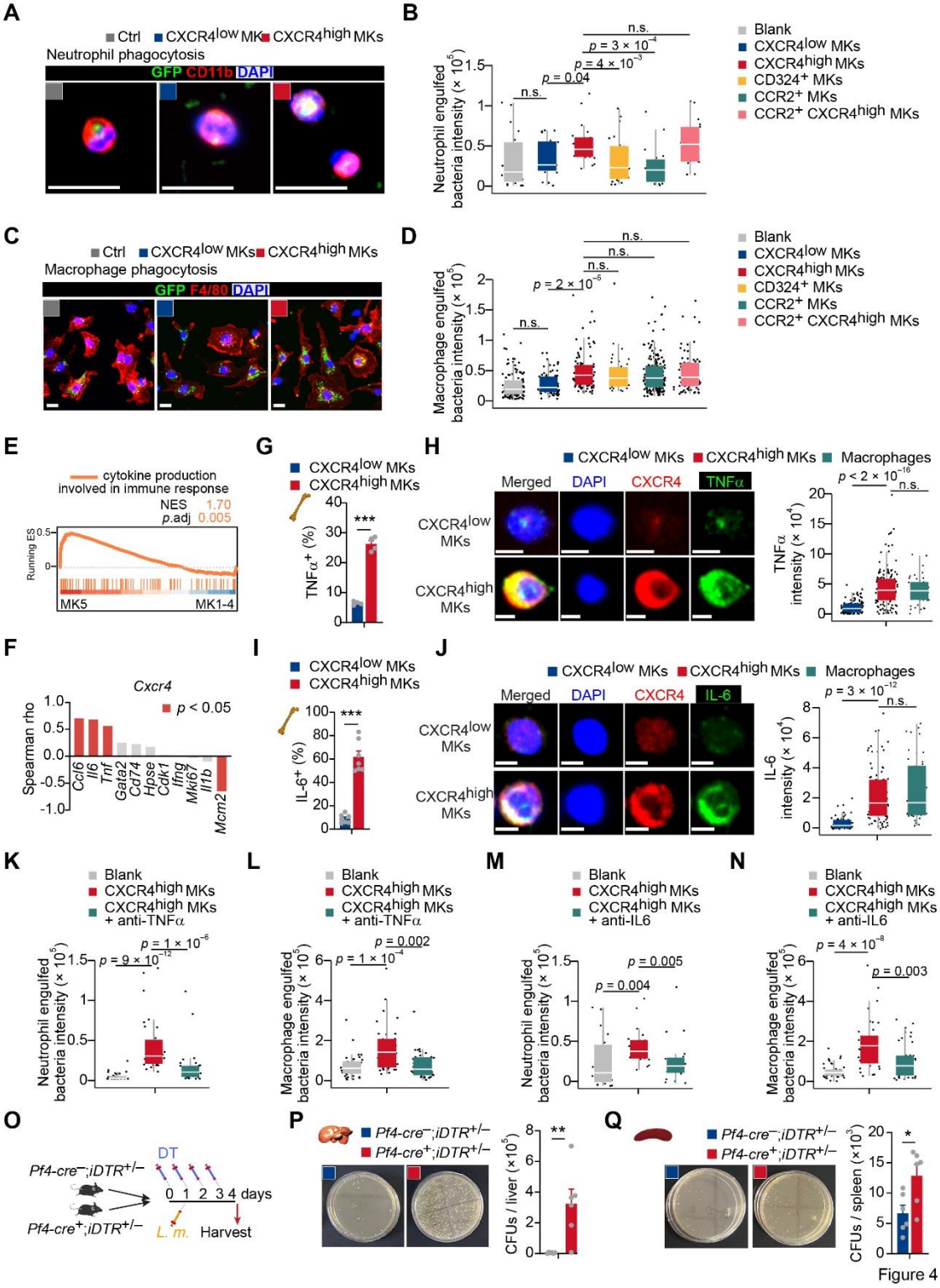
A
Ctrl CXCR4low MK CXCR4high MKs
Neutrophil phagocytosis
GFP CD11b DAPI
B
Neutrophil engulfed bacteria intensity (× 10^5)
n.s.
p = 0.04
p = 4 × 10^-3
p = 3 × 10^-4
Blank
CXCR4low MKs
CXCR4high MKs
CD324+ MKs
CCR2+ MKs
CCR2+ CXCR4high MKs
C
Ctrl CXCR4low MKs CXCR4high MKs
Macrophage phagocytosis
GFP F4/80 DAPI
D
Macrophage engulfed bacteria intensity (× 10^5)
n.s.
p = 2 × 10^-5
E
cytokine production involved in immune response
NES 1.70
p.adj 0.005
Running ES
MK5
MK1-4
G
CXCR4low MKs
CXCR4high MKs
TNFα+ (%)
***
H
CXCR4low MKs CXCR4high MKs Macrophages
Merged DAPI CXCR4 TNFα
CXCR4low MKs
CXCR4high MKs
TNFα intensity (× 10^4)
p < 2 × 10^-16
n.s.
F
Cxcr4
p < 0.05
Spearman rho
Ccl6 Il6 Tnf Gata2 Cd74 Hpse Cdk1 Ifng Mki67 Il1b Mcm2
I
CXCR4low MKs
CXCR4high MKs
IL-6+ (%)
***
J
CXCR4low MKs CXCR4high MKs Macrophages
Merged DAPI CXCR4 IL-6
CXCR4low MKs
CXCR4high MKs
IL-6 intensity (× 10^4)
p = 3 × 10^-12
n.s.
K
Blank
CXCR4high MKs
CXCR4high MKs + anti-TNFα
Neutrophil engulfed bacteria intensity (× 10^5)
p = 9 × 10^-12
p = 1 × 10^-6
L
Blank
CXCR4high MKs
CXCR4high MKs + anti-TNFα
Macrophage engulfed bacteria intensity (× 10^5)
p = 1 × 10^-4
p = 0.002
M
Blank
CXCR4high MKs
CXCR4high MKs + anti-IL6
Neutrophil engulfed bacteria intensity (× 10^5)
p = 0.004
p = 0.005
N
Blank
CXCR4high MKs
CXCR4high MKs + anti-IL6
Macrophage engulfed bacteria intensity (× 10^5)
p = 4 × 10^-8
p = 0.003
O
Pf4-cre−;iDTR+/−
Pf4-cre+;iDTR+/−
DT
0 1 2 3 4 days
L. m.
Harvest
P
Pf4-cre−;iDTR+/−
Pf4-cre+;iDTR+/−
CFUs / liver (×10^5)
**
Q
Pf4-cre−;iDTR+/−
Pf4-cre+;iDTR+/−
CFUs / spleen (×10^5)
*

Figure 4

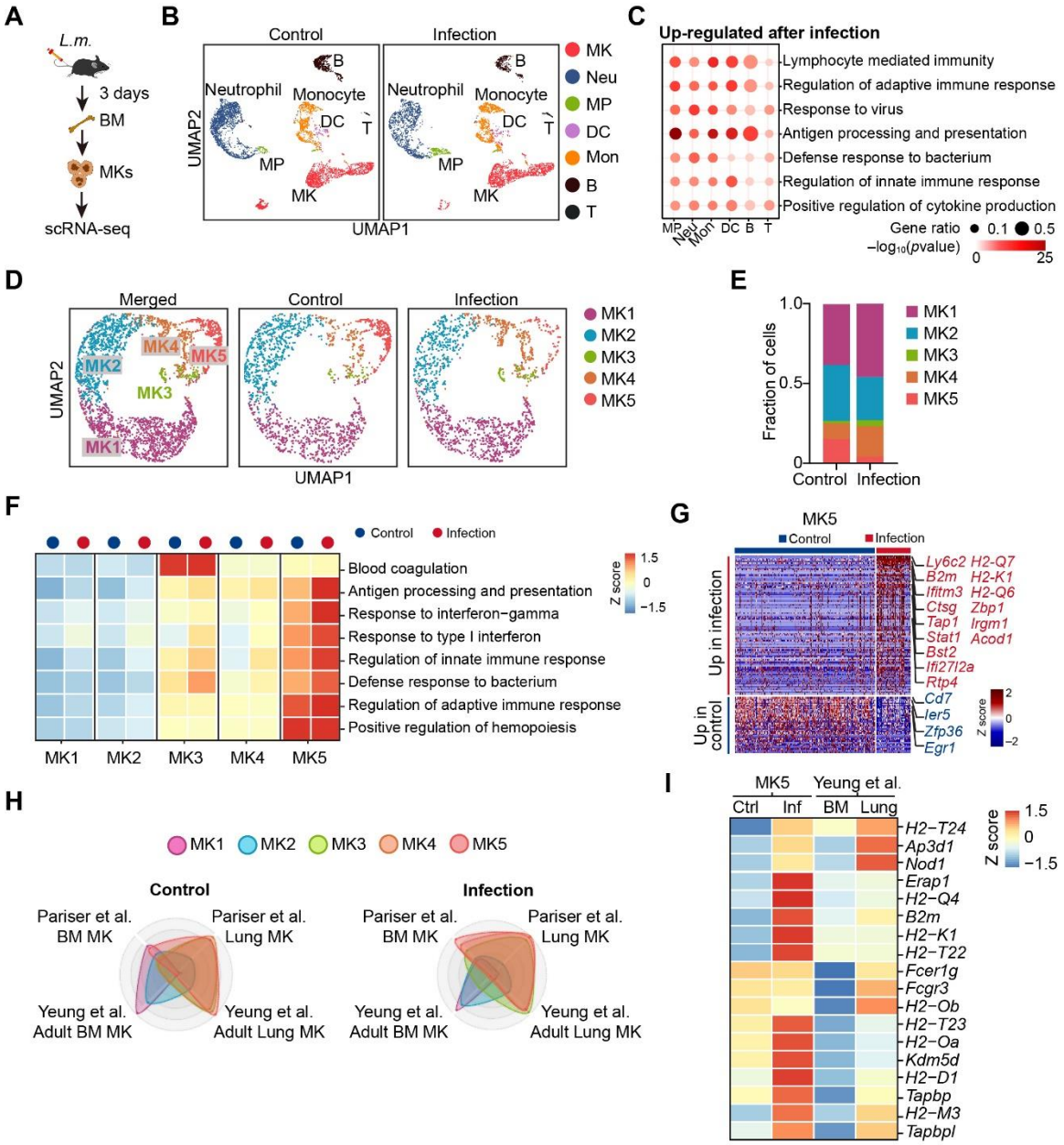
A
L.m.
3 days
BM
MKs
scRNA-seq
B
Control
Infection
Neutrophil
Monocyte
B
DC
T
MP
MK
UMAP2
UMAP1
MK
Neu
MP
DC
Mon
B
T
C
Up-regulated after infection
Lymphocyte mediated immunity
Regulation of adaptive immune response
Response to virus
Antigen processing and presentation
Defense response to bacterium
Regulation of innate immune response
Positive regulation of cytokine production
MP
Neu
Mon
DC
B
T
Gene ratio
0.1
0.5
−log10(pvalue)
0
25
D
Merged
Control
Infection
MK2
MK4
MK5
MK3
MK1
UMAP2
UMAP1
MK1
MK2
MK3
MK4
MK5
E
Fraction of cells
1.0
0.5
0
Control
Infection
MK1
MK2
MK3
MK4
MK5
F
Control
Infection
Blood coagulation
Antigen processing and presentation
Response to interferon−gamma
Response to type I interferon
Regulation of innate immune response
Defense response to bacterium
Regulation of adaptive immune response
Positive regulation of hemopoiesis
Z score
1.5
0
−1.5
MK1
MK2
MK3
MK4
MK5
G
MK5
Control
Infection
Up in infection
Up in control
Ly6c2
H2-Q7
B2m
H2-K1
Ifitm3
H2-Q6
Ctsg
Zbp1
Tap1
Irgm1
Stat1
Acod1
Bst2
Ifi27l2a
Rtp4
Cd7
Ier5
Zfp36
Egr1
Z score
2
0
−2
H
MK1
MK2
MK3
MK4
MK5
Control
Pariser et al. BM MK
Pariser et al. Lung MK
Yeung et al. Adult BM MK
Yeung et al. Adult Lung MK
Infection
Pariser et al. BM MK
Pariser et al. Lung MK
Yeung et al. Adult BM MK
Yeung et al. Adult Lung MK
I
MK5
Yeung et al.
Ctrl
Inf
BM
Lung
H2−T24
Ap3d1
Nod1
Erap1
H2−Q4
B2m
H2−K1
H2−T22
Fcer1g
Fcgr3
H2−Ob
H2−T23
H2−Oa
Kdm5d
H2−D1
Tapbp
H2−M3
Tapbpl
Z score
1.5
0
−1.5

Figure 5

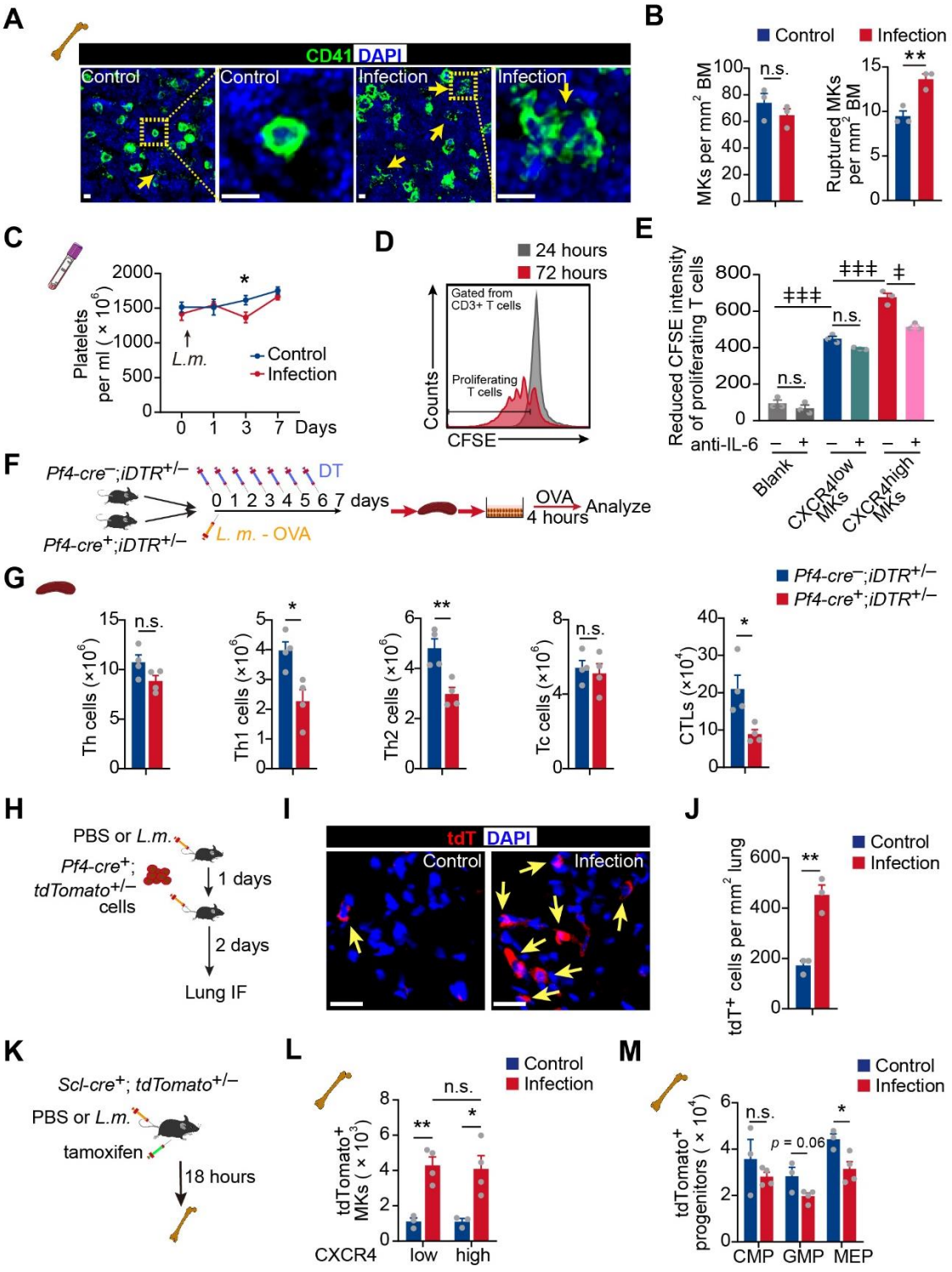
A
CD41 DAPI
Control
Control
Infection
Infection
B
Control
Infection
MKs per mm² BM
n.s.
Ruptured MKs per mm² BM
**
C
Platelets per ml (× 10⁶)
L.m.
Control
Infection
Days
D
24 hours
72 hours
Gated from CD3+ T cells
Proliferating T cells
Counts
CFSE
E
Reduced CFSE intensity of proliferating T cells
anti-IL-6
Blank
CXCR4low MKs
CXCR4high MKs
F
Pf4-cre⁻;iDTR+/–
Pf4-cre+;iDTR+/–
DT
0 1 2 3 4 5 6 7 days
L. m. - OVA
OVA
4 hours
Analyze
G
Pf4-cre⁻;iDTR+/–
Pf4-cre+;iDTR+/–
Th cells (×10⁶)
Th1 cells (×10⁶)
Th2 cells (×10⁶)
Tc cells (×10⁶)
CTLs (×10⁴)
H
PBS or L.m.
Pf4-cre+; tdTomato+/– cells
1 days
2 days
Lung IF
I
tdT DAPI
Control
Infection
J
tdT+ cells per mm² lung
Control
Infection
K
Scl-cre+; tdTomato+/–
PBS or L.m.
tamoxifen
18 hours
L
Control
Infection
tdTomato+ MKs (× 10³)
CXCR4
low
high
M
Control
Infection
tdTomato+ progenitors (× 10⁴)
p = 0.06
CMP
GMP
MEP

Figure 6